# Damage observability, localization and assessment based on eigenfrequencies and eigenvectors curvatures

Jacopo Ciambella, Fabrizio Vestroni* and Stefano Vidoli

*Dipartimento di Ingegneria Strutturale e Geotecnica, Università di Roma "La Sapienza"*
*Via Eudossiana 18, 00184 - Roma, Italy*

**Abstract.**   A technique for damage localization and assessment based on measurements of both eigenvectors curvatures and eigenfrequencies is proposed. The procedure is based on two successive steps: a model independent localization, based on changes of modal curvatures, and the solution of a one-dimensional minimization problem to evaluate damage intensity. The observability properties of damage parameters is discussed and, accordingly, a suitable change of coordinates is introduced. The proposed technique is illustrated with reference to a cantilever Euler beam endowed with a set of piezoelectric transducers. To assess the robustness of the algorithm, a parametric study of the identification errors with respect to the number of transducers and to the number of considered modal quantities is carried out with both clean and noise-corrupted data.

**Keywords:**   damage detection; structural health monitoring; frequency response function; piezoelectric sensors.

## 1. Introduction

Among non-destructive evaluation techniques, vibration-based methods respond to the current tendency which is to integrate identification and monitoring systems in the structure: in an increasing number of projects, transducers and sensors are embedded into the mechanical system and driven by suitably designed electronic controllers.

Over the past two decades, a significant amount of research has been conducted in order to monitor effectively structural health via measurement of the modal response (see, for instance, Doebling *et al*. 1998, Chang *et al*. 2003). Many literature contributions investigated the use of changes in natural frequencies in order to detect damage occurrences (Montalvao *et al.* 2006, and references therein); their feasibility is, however, limited since natural frequencies present a low sensitivity with respect to local variations of the mechanical characteristics. This fact reflects a significant error on the identified parameters as it implies a small curvature of any reasonable functional based on eigenfrequencies (Friswell *et al*. 1994, Friswell and Penny 1997, Morassi and Vestroni 2008).

As a consequence, many researchers have focused their efforts on measuring and using the changes on modal coordinates (Gladwell and Morassi 1999, Lanata and Del Grosso 2006, Mendrok and Uhl 2010). In such cases, the identification of the damage is obtained through the minimization of an objective function dependent on both eigenfrequencies and eigenvectors (see, e.g., Casciati 2008,

*Corresponding Author, Professor, E-mail: vestroni@uniroma1.it

Unger *et al*. 2006, Kim *et al*. 2003, 2007 and references therein). However, it should be remarked that, as soon as the number of unknowns increases, the problem becomes difficult to handle numerically since multiple local minima can appear.

Other techniques proposed were based on measurements of the eigenvectors curvatures; this concept was firstly applied to health monitoring in Pandey *et al*. (1991) and, later, used by many other researchers (Abdel Wahab and De Roeck 1999, Dilena and Morassi 2002, Lestari *et al*. 2007). From a theoretical point of view, it was found to be very promising since the changes of the curvature mode shapes are localized in the region of the damage; however, the difficulties of obtaining reliable measurements of the curvatures had to be faced. In this regard, piezoelectric sensors/actuators glued to the structural surface are an effective and reliable means to measure the structural impedance and thus the curvature of the mode shapes (Park *et al*. 2000, 2003, Park and Inman 2007). Moreover, due to their relative low cost, they allow the use of a distributed network over the entire structure under observation.

In this study, the difference of eigenvectors curvatures and eigenfrequencies between the damaged and the healthy structure is used to localize the damage and assess the damage intensity. The modal curvatures are extracted from the frequency response function (FRF) of the structure as sampled by the piezoelectric patches; because of the properties of this FRF, the proposed method is able to identify both stiffness and mass variation. In this sense, it is an extension of the method proposed in Bernal (2002), which, instead, is based on variation of the flexibility matrix only.

The identification procedure is divided in two successive steps:

1. the localization of damage assessed independently of the model and based on the comparison between undamaged and damaged measured eigenvectors curvatures;
2. the estimate of damage intensity through the minimization of a one-dimensional functional, likely non-convex, based on the comparison between the analytical and measured eigenfrequencies.

This identification technique is illustrated with reference to a cantilever Euler beam, whose model equations are derived in order to evaluate the optimal experimental procedure to assess the frequency response function. Accordingly, the observability properties of the damage descriptors are discussed, suggesting a suitable change of coordinates.

The paper is organized as follows: in Section 2 the equations of motion for an Euler beam coupled with a set of distributed piezoelectric patches are derived. In Section 3 the damage model and the identification procedure are presented and discussed. In Section 4 two numerical examples are presented and the main conclusions are outlined. Finally, the Appendix includes a proof of the non-observability of the damage local shape for moderate damage intensities.

## 2. System description and model equations

A cantilever beam hosting a uniformly distributed array of piezoelectric transducers is considered (Fig. 1).
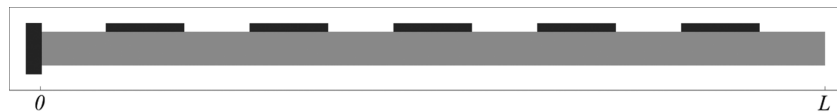


Fig. 1 Cantilever electromechanical beam of length *L* endowed with 5 piezoelectric patches

In dell'Isola *et al.* (2004) the evolution equations of an electromechanical beam are derived. Applying those results, the state of the system can be described by the scalar field, $w(x, t)$, representing the transverse deflection of the beam axis, and by the vector of nodal flux linkages at the terminals of the $N$ piezoelectric transducers; the flux linkage $\psi_i$ is the time integral of the nodal voltage $V_i$, e.g., $V_i = \dot{\psi}_i$. When a mechanical excitation $f(x, t)$ is applied, the discrete evolution equations of the coupled system, obtained by means of a standard modal projection, are

$$\begin{cases} K_{\alpha\beta}(\pi)W_\beta(t) + C_{\alpha\beta}\dot{W}_\beta(t) + M_{\alpha\beta}\ddot{W}_\beta(t) + \Gamma_{\alpha i}\psi_i(t) = F_\alpha(t) \\ Y_{ij}\psi_j(t) + R_{ij}\dot{\psi}_j(t) + B_{ij}\ddot{\psi}_j(t) - \Gamma_{\alpha i}\dot{W}_\alpha(t) = Q_i(t) \end{cases} \tag{1}$$

where $t$ denotes the time variable and a superimposed dot indicates the time derivative; hereafter the sum over repeated indices is omitted. Here $j = 1,...N$ and $\alpha, \beta = 1,..., A$, being $A$ the dimension of the chosen basis.

In Eq. (1) $W_\alpha$ is the projection of the displacement field and represents the mechanical degrees of freedom, whilst $\psi_j$ is the electrical counterpart. Correspondingly, **K**, **C**, **M** and **Y**, **R**, **B** can be interpreted as the stiffness, damping and mass matrices for the two subsystems, whilst **F** and **Q** are the external applied actions. The stiffness matrix **K** explicitly depends on the material and geometrical constitutive quantities which are here assumed as monitored parameters and collected in the vector $\pi$. The matrix $\Gamma$ models the gyroscopic coupling between the structure and the electrical system.

By means of Laplace transform, solving (1.1) for the vector **W** and replacing in (1.2), one gets

$$(Y_{ij} + sR_{ij} + s^2 B_{ij})\tilde{\psi}_j + s^2\Gamma_{\alpha i}H_{\alpha\beta}(s, \pi)\Gamma_{\beta j}\tilde{\psi}_j = \overline{Q}_i - s\Gamma_{\alpha i}\overline{F}_\alpha \tag{2}$$

where $s$ is the Laplace variable and a superimposed tilde means the Laplace transform of the corresponding time function; The quantities $\overline{Q}_i$ and $\overline{F}_\alpha$ represent the electrical and mechanical initial conditions while the matrix $H(s, \pi) := [K(\pi) + sC + s^2 M]^{-1}$ is the frequency response of the mechanical system. This algebraic manipulation establishes an explicit relationship between the flux linkages $\tilde{\psi}$ and the electrical currents $\overline{Q}$.

By considering Eq. (2) with vanishing initial conditions and vanishing applied forces, the Frequency Response Function (FRF) of the whole structure can be defined, viz.

$$N_{ij}(s,\pi) := Y_{ij} + sR_{ij} + s^2 B_{ij} + s^2\Gamma_{\alpha i} H_{\alpha\beta}(s, \pi)\Gamma_{\beta j} \tag{3}$$

$$N_{ij}(s, \pi)\tilde{\psi}_j = \tilde{Q}_i \tag{4}$$

From an experimental point of view, the aquisition of the FRF $N_{ij}(s)$ requires an electronic interface circuit able to impose a suitable current on each PZT patch while measuring the voltages $\dot{\psi}_i$. This FRF is represented as the sum of the purely electric admittance, independent of the monitored parameters $\pi$, plus the function

$$D_{ij}(s, \pi) := s^2\Gamma_{\alpha i}H_{\alpha\beta}(s, \pi)\Gamma_{\beta j} \tag{5}$$

which can be physically interpreted as the additional admittance measured in the electric system, due to its coupling with the structure. Moreover, it follows that the additional mechanical impedance $D_{ij}(s, \pi)$:
- is experimentally obtained as a difference between the frequency response $N_{ij}(s, \pi)$ and the purely electric impedance $N_0(s) = \mathbf{Y} + s\mathbf{R} + s^2\mathbf{B}$;
- is independent of the electric parameters **Y**, **R** and **B**;

- contains information on mechanical eigenfrequencies and eigenvectors only.

More precisely, using the spectral decomposition of the mechanical frequency response function, i.e.,

$$H_{\alpha\beta}(s,\pi) := \sum_{h=1}^{\infty} \frac{u_\alpha^{(h)} u_\beta^{(h)}}{s^2 + \varpi_h^2 + 2s\delta_h\varpi_h} \tag{6}$$

one obtains the following representation of the additional mechanical impedance in terms of mechanical eigenvectors $\{u^{(h)}\}_{h=1}^{N}$ and eigenfrequencies $\{\varpi_h\}_{h=1}^{N}$

$$D_{ij}(s,\pi) = s^2 \sum_{h=1}^{\infty} \frac{z_i^{(h)} z_j^{(h)}}{s^2 + \varpi_h^2 + 2s\delta_h\varpi_h}, \quad z_i^{(h)} := \sum_\alpha \Gamma_{\alpha i} u_\alpha^{(h)} \tag{7}$$

being $\delta_h$ the damping coefficient associated with the $h$-th eigenfrequency. The eigenvectors $z_i^{(h)}$ of the matrix $D_{ij}$ are the mode shape curvatures as sampled by the PZT patches through the coupling matrix $\Gamma$. The above-mentioned properties of the function $D$ are used in the following for the proposed identification technique.

## 3. Identification procedure

### 3.1 Damage model and observability

In order to assess the observability of damage parameters, a model for the stiffness variation has to be introduced. To this end, the structural domain is decomposed as the union of $H$ regions (possibly according to the position of the PZT transducers).

The bending stiffness $k(\pi, x)$ is expressed as follows

$$k(\pi, x) = k_0(x) - \Delta k(\pi, x) = k_0(x) - \sum_{h=1}^{H} d_h f_h(G_h, b_h; x) \tag{8}$$
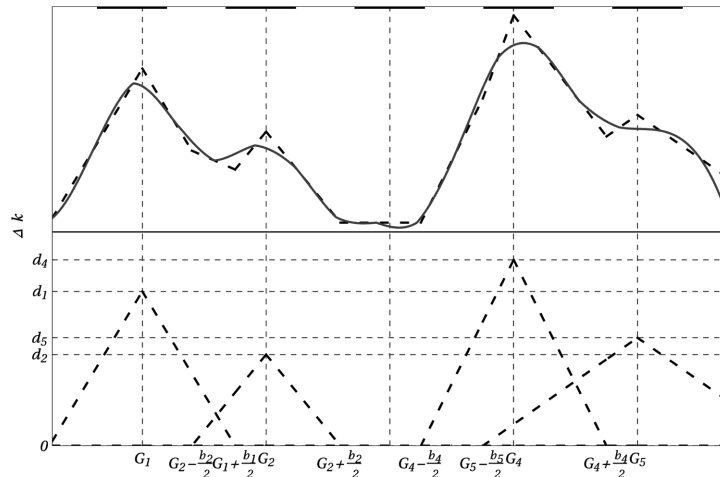


Fig. 2 Damage parametrization through triangular shaped functions. The top figure represents the actual damage scenario (continuous gray line) and its interpolation through a linear function (dashed black line); the bottom figure depicts the interpolating triangular shaped functions

where $f_h(G_h, b_h; x)$ are piecewise linear functions having values 1 in the centroids $G_h$ of the $H$ regions and vanishing outside the $h$-th interval $I_h = [G_h - b_h/2, \; G_h + b_h/2]$ (see Fig. 2); namely, it results

$$f_h(G_h, b_h; x) = \begin{cases} 2\dfrac{x-G_h}{b_h}+1, & G_h - b_h/2 \le x < G_h, \\[2mm] 1+2\dfrac{G_h-x}{b_h}, & G_h \le x < G_h + b_h/2, \\[2mm] 0, & x < G_h - b_h/2 \quad \text{or} \quad x \ge G_h + b_h/2, \end{cases}$$

being, for each $h$, $d_h < \min_{x \in [0, L]} k_0(x)$, to assure the positivity of the bending stiffness. This parametrization is effective in representing the circumstance of concentrated damages.

The $2H$ scalar quantities $\{b_1, b_2,...,b_H\}$ and $\{d_1, d_2,...,d_H\}$ represent the damage widths and depths in each of the $H$ regions respectively; these quantities define the introduced function $\Delta k$ and are the actual unknowns of the identification procedure. It should be noted that the parameters $b_h$ are independent of the distance among the centroids $G_h$.

Through the change of coordinates

$$\begin{cases} A_h = d_h b_h, \\ r_h = d_h/b_h, \end{cases} \quad \begin{cases} d_h = \sqrt{A_h r_h} \\ b_h = \sqrt{A_h/r_h} \end{cases} \tag{9}$$

each damage $\{b_h, d_h\}$ can be expressed in terms of intensity $A_h$ and local shape $r_h$. Such a change of coordinates turns out to be useful to investigate the observability of the damage parameters. Indeed, it is proved in the Appendix that, for moderate damage intensities, the sensitivity of the FRF $D$ with respect to the damage shape parameters $r$ vanishes, namely

$$\lim_{\|A\|_\infty \to 0} \frac{\left\| \dfrac{\partial}{\partial r} D(A, r) \right\|_\infty}{\left\| \dfrac{\partial}{\partial A} D(A, r) \right\|_\infty} = 0 \tag{10}$$

being $\|A_h\|_\infty = \sup_h |A_h|$ and $\|C_{ijk}\|_\infty = \sup_{i,j,k}|C_{ijk}|$.

Eq. (10) states that in the case of small damage intensities ($\|A\|_\infty \to 0$), the frequency response function $D$ is much more sensitive to variation of the damage parameters $A$ than to variation of the damage shapes $r$. Since the technical interest is focused on small damage intensities, the damage local shapes can be excluded from the analysis. As a consequence, the identification procedure is reduced to the choice of a suitable functional to be minimized on the space of unknowns $\pi = A$, i.e.,

$$A^* = \mathrm{argmin}_A F(A) \tag{11}$$

where $\mathrm{argmin}_A F(A)$ is the vector where the minimum of the functional is attained.

A common choice for $F(A)$ is based on differences of eigenfrequencies (Doebling *et al.* 1998, Vestroni and Capecchi 2000), i.e.,

$$F(A) = \left\| \varpi(A) - \varpi^* \right\| \tag{12}$$

where $\varpi(A) = \{\varpi_1(A), ..., \varpi_M(A)\}$ are the first $M$ eigenfrequencies of the model (1) in the damaged state $A$, while $\varpi^* = \{\varpi_1^*, ..., \varpi_M^*\}$ are the corresponding measured quantities.

The functional $F(A)$ is generally non-convex, hence, in performing its minimization, several local minima can be found: as the dimension of the damage vector $A$ grows, the problem can easily become untreatable. The non-convexity of $F(A)$ is observed since the sign of the matrix $\Delta K = K(A) - K^*$, meaning the difference between the current model stiffness associate to $A$ and the actual damaged stiffness, is generally not definite.

## 3.2 Damage localization and assessment

In order to avoid numerical difficulties in the minimization of a non-convex functional $F(A)$, a reduced version of the minimization problem (11) is introduced. Accordingly, the identification of the unknown vector $A$ is split into the estimate of the actual damage shape $a$ ($a = \alpha^{-1}A$ with $\alpha = \|A\|$) and thereafter of the damage scale $\alpha$.

It is interesting to introduce a procedure for the estimate of $a$, which can be obtained independently of the model by using only the differences on the eigenvectors curvatures extracted from the measurements of damaged $D_{ij}^*$ and undamaged $D_{ij}^0$ FRFs. Actually, as far as beam structures are concerned, this approach is related to the measurements of the nodal points (see, e.g., Gladwell and Morassi 1999, Dilena and Morassi 2002). However, only the method based on the measurements of eigenvector curvature can be readily extended to two-dimensional structures.

The proposed approach strongly relies on the assumption that large eigenvectors differences are essentially localized in the damaged regions. Moreover, it is assumed that the PZT patches are uniformly distributed over the entire structural members under observation.

Eq. (7) highlights the dependence of the FRF $D$ on the modal shape curvatures in the measured frequency range. Hence, standard techniques can be used to estimate the undamaged eigenvectors curvatures $\{z_0^{(1)}, ..., z_0^{(M)}\}$, derived from $D^0$, and the damaged eigenvectors curvatures $\{z_*^{(1)}, ..., z_*^{(M)}\}$, derived from $D^*$.

Once the modal shapes curvatures are extracted, the following procedure allows the overall damage shape $a^*$ to be identified robustly.

(a) The average difference between eigenvector curvatures is defined as

$$v = \frac{1}{M}\sum_{m=1}^{M}\left|\overline{z}_*^{(M)} - \overline{z}_0^{(M)}\right| \tag{13}$$

where $\overline{z}_*$, $\overline{z}_0$ are the normalized eigenvectors and $M$ is the number of measured eigenfrequencies. The vector $v$ is equivalent to the Curvature Damage Factor (CDF) introduced by Abdel Wahab and De Roeck (1999) (see also Lestari *et al.* 2007).

(b) All the maxima exceeding a selected threshold $s$ are considered. This step allows the inessential local peaks to be filtered out by selecting the regions where a relevant stiffness variation actually occurs.

(c) Each relevant peak is interpolated by means of triangular shape function which strictly contains the vector $v$.

(d) The triangles obtained allow the vector $a^*$ to be estimated. Patches corresponding to nonzero values $(a^*)_i$ are assumed to correspond to damaged regions.

As it will be shown in the next section through numerical examples, the aforementioned procedure allows a set of localized stiffness variations to be robustly identified. While step (b) is used to filter out the possible numerical noise on the signal, step (d) makes the sign of the difference between the extrapolated and the actual stiffness variation, at least, locally definite. The triangular shape function

used in step (c) could suggest a possible choice of the damage shape vector *r*.

The procedure relies on the assumption of localized stiffness variations, which is the case more frequently dealt with, but could be extended to the case of distributed stiffness variations. Once the unit vector $a^*$ has been estimated, the identification problem (11) is reduced to

$$\alpha^* = argmin_{\alpha \in \mathbb{R}} F(\alpha, a^*) \tag{14}$$

which is a one-dimensional minimization problem and, consequently, the non-convexity of $F$ can be easily accounted for. Furthermore, being the functional $F$ based on eigenfrequencies only, a minimal model of the structure is sufficient.

## 4. Numerical examples

To illustrate the effectiveness of the proposed identification algorithm a cantilever beam with 3, 5, 10 and 20 PZT patches is considered (see Fig. 1 for the case of 5 PZT).

The beam is clamped at $x = 0$ and the free end is located at $x = L$. The PZT sensors are equally spaced along the beam length; while the number of the patches is increased, the covering ratio $c_R$, i.e., the ratio between the length covered by the transducers and total length $L$, is held constant ($c_R = 0.5$). The overall system is governed by Eq. (1).

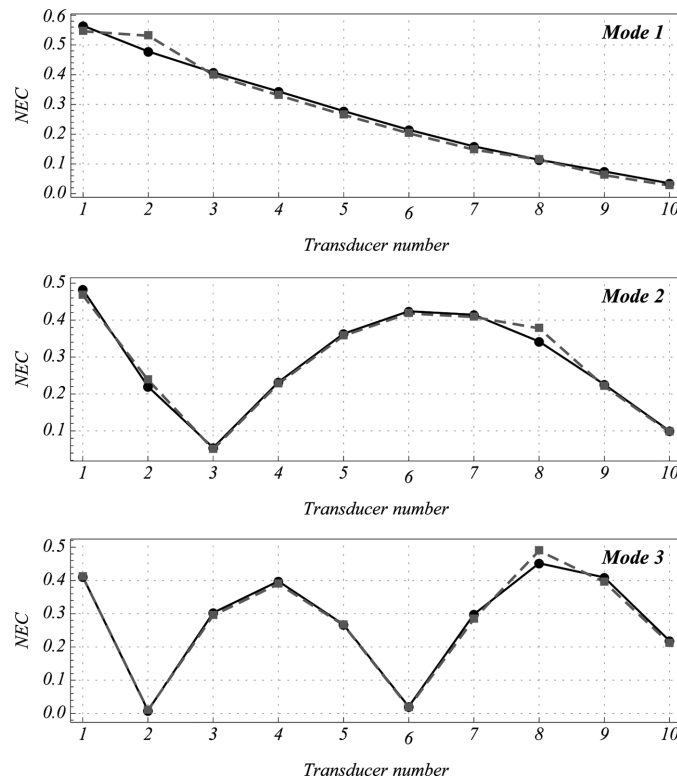The case of a beam with 2 damages is considered; in particular it is assumed that $x_1 = 0.16$,



Fig. 3 Normalized Eigenvectors Curvatures (*NEC*) of the FRF $D^0$ (continuous) and $D^*$ (dashed) as sampled by 10 PZT transducers for the considered damage case

$b_1 = 0.10$ and $d_1 = 0.25$ while $x_2 = 0.68$, $b_2 = 0.15$ and $d_2 = 0.15$; these data correspond to damage areas $A_1 = d_1 b_1 = 2.50\%$ and $A_2 = d_2 b_2 = 2.25\%$. The actual stiffness reduction is represented as a solid gray line in Fig. 5.

Fig. 3 represents the normalized eigenvectors curvatures of the first three eigenmodes in the case of 10 PZT patches for the undamaged and damaged state. Since the PZT transducers naturally sense the modal curvatures, the first eigenmode is much more sensitive to damage occurrences near the clamp, while the sensitivities of higher order eigenvectors are localized in the regions where their maximal curvatures occur.

The localization procedure introduced in the previous section furnishes the undamaged and damaged shapes and allows the estimate of the unit vector $\boldsymbol{a}^*$, which represents the nondimensional stiffness distribution along the beam. In particular, in Fig. 4, the vector $\boldsymbol{v}$ and the corresponding triangular shape functions computed through steps (a)-(e) in the case of 5 patches and 3 eigenmodes are displayed. By means of the filtering procedure, the region where the differences between elements of $\boldsymbol{v}$ are minima is recovered and corresponds, in the present case, to the 2nd and 3rd PZT patches. The vector $\boldsymbol{a}^*$ is obtained by interpolating $\boldsymbol{v}$ with two triangular shape functions; all the minima below the threshold, represented as a grey region in the figure, are discarded.

By using the difference in the eigenfrequencies, the reduced minimization problem (14) is solved and, therefore, the damage intensity $\alpha^*$ is obtained.

The identification results are reported in Fig. 5 for an increasing number of PZT patches (3, 5, 10, 20) and for a different number of considered modes (1, 2, 3), while Table 1 lists the resulting percentage errors in the estimate of damage positions and intensities. Here, the identified damage position is assumed in the abscissa where the maximum of the vector $\boldsymbol{a}^*$ is attained, which depend on the PZT distribution. In particular, for the cases of 3 and 5 PZT patches, the first maximum in $\boldsymbol{a}^*$ was attained in correspondence of the first patch, which in both cases was centered at $x/L = 0.13$; as a consequence, the relative error in the localization of the first damage was the same as reported in Table 1.

As expected, a prelocalization based only on the first eigenmode cannot detect a damage located at $x = 0.68$, since it occurs in a small curvature region and is filtered out by the signal processing procedure. From the results shown in Fig. 5 and in Table 1, the following observations can be made:

1. as the number of PZT patches increases the percentage error on the damage position decreases;
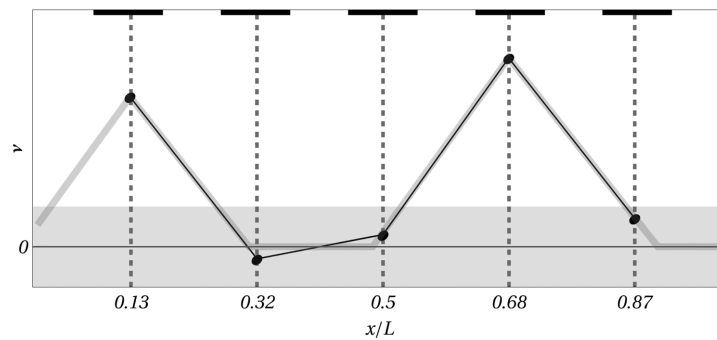


Fig. 4 Filtering procedure applied to the difference of eigenvectors curvature $\boldsymbol{v}$ (dotted black line). The thick gray line is the vector $\boldsymbol{a}^*$ resulting from the procedure sketched in steps (a)-(d). The figure refers to the case of 5 PZT patches and 3 eigenmodes; the abscissa of the center of each patch is highlighted in the figure
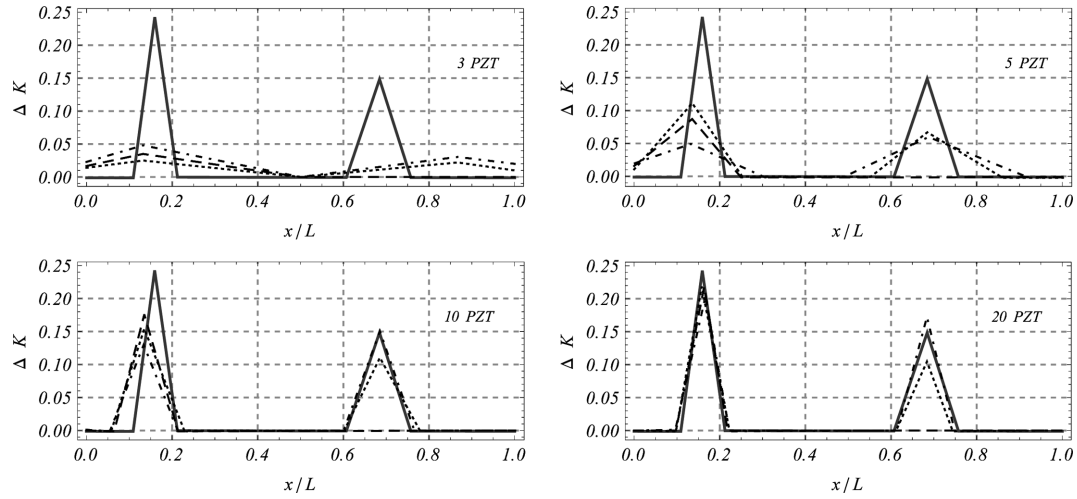
Fig. 5 Estimated stiffness reduction *ΔK* for an increasing number of PZT patches and of eigenvectors used in the identification procedure (actual stiffness variation - continuous line, 1 eigenvector - dashed, 2 eigenvectors - dotted, 3 eigenvectors - dot dashed)

Table 1 Results of the proposed identification procedure for an increasing number of PZT patches and eigenmodes

| PZT Num. | | Actual param. | | 1 mode Error (%) | | 2 modes Error (%) | | 3 modes Error (%) | |
|---|---|---|---|---|---|---|---|---|---|
| | | Pos. | Area (%) | Pos. | Area (%) | Pos. | Area (%) | Pos. | Area (%) |
| 3 | D1 | 0.16 | 2.50 | -15.8 | 18.13 | -15.8 | -4.91 | -15.8 | 17.9 |
| | D2 | 0.68 | 2.25 | - | - | 28.1 | -52.1 | 28.1 | -28.0 |
| 5 | D1 | 0.16 | 2.50 | -15.8 | 8.3 | -15.8 | 6.0 | -15.8 | 4.3 |
| | D2 | 0.68 | 2.25 | - | - | 0.0 | -10.5 | 0.0 | 16.4 |
| 10 | D1 | 0.16 | 2.50 | -9.5 | 9.9 | -9.5 | 9.3 | -9.5 | -7.3 |
| | D2 | 0.68 | 2.25 | - | - | 0.0 | -12.9 | 0.0 | 10.8 |
| 20 | D1 | 0.16 | 2.50 | 5.3 | -2.3 | -1.3 | 3.0 | 5.3 | 2.9 |
| | D2 | 0.68 | 2.25 | - | - | 0.0 | -13.1 | 0.0 | 3.4 |

   2. an accurate estimate of damage intensities can be achieved even with the smallest number of PZT patches; however, with 10 or 20 patches the damage shapes are much more accurately estimated;

   3. the damage intensity estimate is also improved by considering an increasing number of eigenmodes.

   In the case of two damages considered, the ratio between the two areas $A_1$ and $A_2$ can be computed from $\boldsymbol{a}^*$.

   Fig. 6 shows, in the plane $A_1A_2$, the refinement in the estimate of the actual damage parameters $\boldsymbol{a}^*$ and $A^*$ produced by an increasing number of PZT transducers. The case of only 3 PZT gives a direction in the plane $A_1A_2$ which leads to a solution of the minimization problem ($A_{III}$) significantly far from the exact minimum. On the contrary, the solution with 20 PZT patches ($A_{XX}$) is essentially the same of the actual minimum. In addition, from the position of minima $A_{III}$, $A_V$, $A_X$ and $A_{XX}$ in Fig. 6, the convergence of the proposed procedure with respect to the increasing number of PZT patches can be appreciated.
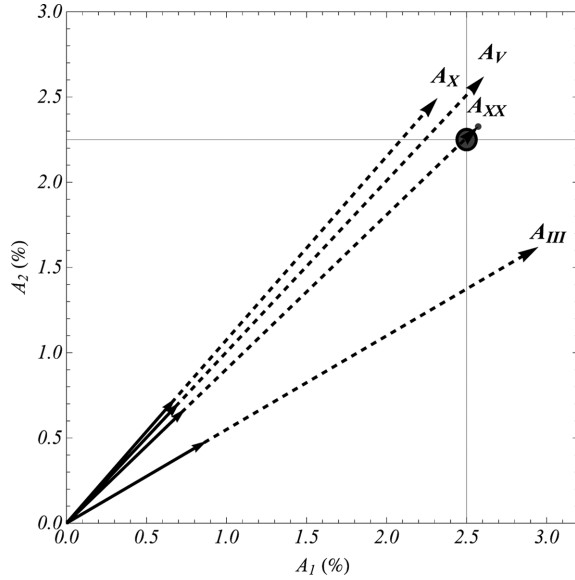
Fig. 6 Refinement in the estimate of the actual damage parameters $A^*$ (gray disk in the plot) produced by an increasing number of PZT considered ($A_{III}$ - 3 PZT, $A_V$ - 5 PZT, $A_X$ - 10 PZT, $A_{XX}$ - 20 PZT). All the results refer to the case of $M=3$ eigenvectors used in the identification procedure
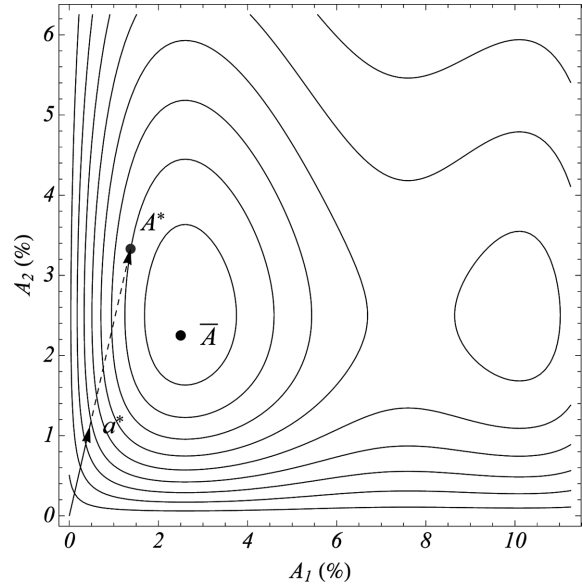
Fig. 7 Contour plot of the functional $F(A)$ in the case of $H=2$ regions. The estimated unit vector $a^*$, the estimated damage vector $A^* = \alpha^* a^*$ and the actual global minimum $\overline{A}$ are shown

Table 2 Sensitivity of the proposed identification procedure with respect to measurement errors for different error level and in the case of 2 eigenmodes and 10 PZT patches considered

| Noise-to-signal-ratio | | 1% | | 5% | | 10% | |
|---|---|---|---|---|---|---|---|
| | | D1 | D2 | D1 | D2 | D1 | D2 |
| Error (%) | Pos. | -9.5 | 0.0 | -9.5 | 0.0 | -9.5 | 0.0 |
| | Area | 9.3 | -12.9 | 9.7 | -9.9 | 11.0 | -11.5 |

The contour plot of the functional $F(A)$ for the simplest case of 2 PZT transducers and $H=2$ regions is drawn in Fig. 7. The result plotted underlines the advantages of the proposed procedure; indeed, the difficulties related to the presence of two local minima are overcome by the introduction of the localization process, i.e., by the estimate of the unit vector $a^*$, which does not rely on any model for the structure, but it is obtained only from the experimental measurements of the eigenvectors. In any case it should be remarked that the value $A^*$, as identified by the proposed procedure, represents a good starting point to minimize the functional $F(\mathbf{A})$ without constraints, being located in the region of the actual minimum of $F(A)$.

Finally, random noise with Gaussian distribution and 1%, 5% and 10% Noise-to-Signal Ratio (NSR) is added to each component of the matrix $D_{ij}$. The main objective of this numerical setup is to assess the robustness of the proposed procedure with respect to measurement errors; the corresponding results are shown in Table 2. For increasing NSR, there is a slight change in the estimate of resonant frequencies, which suggests change in the stiffness of the structure and leads to errors on the area estimate. On the opposite, the location of damage is clearly identified, even with

noisy data. This is essentially due to the filtering procedure introduced which allows the random noise with zero mean level to be filtered out.

## 5. Conclusions

A procedure for the identification of multiple lumped damages in beam-like structures is presented. It is divided into two successive steps, i.e., the estimate of the overall damage shape $a^*$ and the correct scale of the overall damage intensity $\alpha^*$. The localization step is model independent, whilst the damage assessment step uses minimal information from the structural model, being based only on a small number of its eigenfrequencies.

The computational effort of solving a global minimization problem of a non-convex functional of several variables is, hence, reduced to a simple one-dimensional problem. To verify the robustness of the procedure with respect to experimental errors, an analysis using noisy data is carried out.

The results of the numerical simulations have shown a good agreement between the estimated and the actual damage scenario. However, the estimate of the position is much sensitive to the distribution of PZT patches and, in particular, to the position of the patches relatively to the position of damage. In this regard, the quality of the identification drastically improves as the number of sensors increases and their size decreases. This, actually, allows a more accurate sampling of the eigenvectors curvature to be achieved.

From a technological point of view, since the procedure relies on a sampling of the modal shapes curvatures by means of piezoelectric transducers, it can be easily extended to more complex multi-dimensional structures.

## Acknowledgements

## References

Abdel Wahab, M.M. and Roeck, G. D. (1999), "Damage detection in bridges using modal curvatures: application to a real damage scenario", *J. Sound Vib*., **226**(2), 217-235.

Bernal, D. (2002), "Load vectors for damage localization", *J. Eng. Mech.- ASCE*, **128**(1), 7-14.

Casciati, S. (2008), "Stiffness identification and damage localization via differential evolution algorithms", *Struct. Health Monit*., **15**(3), 436-449.

Chang, P.C., Flatau, A. and Liu, S.C. (2003), "Review paper: health monitoring of civil infrastructure", *Struct. Health Monit*., **2**(3), 257-267.

Dell'Isola, F., Maurini, C. and Porfiri, M. (2004), "Passive damping of beam vibrations through distributed electric networks and piezoelectric transducers: prototype design and experimental validation", *Smart Mater. Struct*., **13**(2), 299-308.

Dilena, M. and Morassi, A. (2002), "Identification of crack location in vibrating beams from changes in node positions", *J. Sound Vib*., **255**(5), 915-930.

Doebling, S.W., Farrar, C.R. and Prime, M.B. (1998). "A summary review of vibration-based damage identification methods", Identification Methods, *Shock Vib*., **30**, 91-105.

Friswell, M.I. and Penny, J.E.T. (1997), "Is damage location using vibration measurements practical?", *Proceedings of the EUROMECH 365 International Workshop: DAMAS97, Structural Damage Assessment Using Advanced Signal Processing Procedures*, Sheffield, UK.

Friswell, M.I., Penny, J.E.T. and Wilson, D.A.L. (1994), "Using vibration data and statistical measures to locate damage in structures", *J. Analytical and Experimental Modal Analysis*, **9**(4), 239-254.

Gladwell, G.M.L. and Morassi, A. (1999), "Estimating damage in a rod from changes in node positions", *Inverse Probl.*, **7**(3), 215-233.

Kim, J.T., Park, J.H., Yoon, H.S. and Yi, J.H. (2007), "Vibration-based damage detection in beams using genetic algorithm", *Smart Struct. Syst.*, **3**(3), 263-280.

Kim, J.T., Ryu, Y.S., Cho, H.M. and Stubbs, N. (2003), "Damage identification in beam-type structures: frequency based method vs mode-shape-based method", *Eng. Struct.*, **25**(1), 57-67.

Lanata, F. and Del Grosso, A. (2006), "Damage detection and localization for continuous static monitoring of structures using a proper orthogonal decomposition of signals", *Smart Mater. Struct.*, **15**(6), 1811-1829.

Lestari, W., Qiao, P. and Hanagud, S. (2007), "Curvature mode shape-based damage assessment of carbon/epoxy composite beams", *J. Intel. Mat. Syst. Struct.*, **18**(3), 189-208.

Mendrok, K. and Uhl, T. (2010), "The application of modal filters for damage detection", *Smart Struct. Syst.*, **6**(2), 115-133.

Montalvao, D., Maia, N.M.M. and Ribeiro, A.M.R. (2006), "A review of vibration-based structural health monitoring with special emphasis on composite materials", *Shock Vib.*, **38**(4), 295-324.

Morassi, A. and Vestroni, F. (2008), "Dynamic methods for damage detection in structures", Number 499 in CISM International Centre for Mechanical Sciences. Springer.

Pandey, A.K., Biswas, M. and Samman, M.M. (1991), "Damage detection from changes in curvature mode shapes", *J. Sound Vib.*, **145**(2), 321-332.

Park, G., Cudney, H.H. and Inman, D.J. (2000), "An integrated health monitoring technique using structural impedance sensors", *J. Intel. Mat. Syst. Struct.*, **11**(6), 448-455.

Park, G. and Inman, D.J. (2007), "Structural health monitoring using piezoelectric impedance measurements", *Philos.T. R. Soc. A.*, **365**(1851), 373-392.

Park, G., Sohn, H., Farrar, C.R. and Inman, D.J. (2003), "Overview of piezoelectric impedance-based health monitoring and path forward", *Shock Vib.*, **35**(6), 451-463.

Unger, J.F., Teughels, A. and Roeck, G.D. (2006), "System identification and damage detection of a prestressed concrete beam", *J. Struct. Eng.-ASCE*, **132**(11), 1691-1698.

Vestroni, F. and Capecchi, D. (2000), "Damage detection in beam structures based on frequency measurements", *J. Eng. Mech.-ASCE*, **126**(7), 761-768.

*FC*

## Appendix A

### A-1. Independence of the FRF on the damage shape

Here we prove that for moderate damage intensities ($\|\boldsymbol{A}\|_\infty \to 0$) the sensitivity of the FRF $D$ (Eq. 5) with respect to damage local shape $\boldsymbol{r}$ is vanishing, i.e.,

$$\lim_{\|A\|_\infty \to 0} \frac{\left\|\dfrac{\partial}{\partial \boldsymbol{r}} D(\boldsymbol{A},\boldsymbol{r})\right\|_\infty}{\left\|\dfrac{\partial}{\partial \boldsymbol{A}} D(\boldsymbol{A},\boldsymbol{r})\right\|_\infty} = 0 \tag{15}$$

In this context, it is useful to recall the expression of the additional admittance (5)

$$D_{ij}(\boldsymbol{A},\boldsymbol{r}) := s^2 \Gamma_{\alpha i} D_{\alpha\beta}(\boldsymbol{A},\boldsymbol{r}) \Gamma_{\beta j} \tag{16}$$

where

$$H_{\alpha\beta}(\boldsymbol{A},\boldsymbol{r}) := \{[\boldsymbol{K}(\boldsymbol{A},\boldsymbol{r}) + s\boldsymbol{C} + s^2 \boldsymbol{M}]^{-1}\}_{\alpha\beta} \tag{17}$$

By applying the change of coordinates (9) and using the chain rules, the derivatives of the FRF with respect to the *h*-th damage components are

$$\left|\frac{\partial D_{ij}}{\partial r_h}\right| = \left|\hat{H}_{i\gamma} \left(\frac{\partial K_{\gamma\delta}}{\partial b_k}\frac{\partial b_k}{\partial r_h} + \frac{\partial K_{\gamma\delta}}{\partial d_k}\frac{\partial d_k}{\partial r_h}\right)\hat{H}_{j\delta}\right|$$

$$\left|\frac{\partial D_{ij}}{\partial A_h}\right| = \left|\hat{H}_{i\gamma} \left(\frac{\partial K_{\gamma\delta}}{\partial b_k}\frac{\partial b_k}{\partial A_h} + \frac{\partial K_{\gamma\delta}}{\partial d_k}\frac{\partial d_k}{\partial A_h}\right)\hat{H}_{j\delta}\right| \tag{18}$$

where $\hat{H}_{i\gamma} = s\Gamma_{\alpha i} H_{\alpha\gamma}(\boldsymbol{A},\boldsymbol{r})$.

Since the stiffness variation between the undamaged and damaged system is $\Delta K_{\gamma\delta}(\boldsymbol{A},\boldsymbol{r}) = K_{\gamma\delta}(\boldsymbol{A},\boldsymbol{r}) - K_{\gamma\delta}(\boldsymbol{A}^0,\boldsymbol{r}^0)$, it can be expressed with a standard modal projection through the modal shape functions $\phi_\delta''$, e.g.,

$$\Delta K_{\gamma\delta}(d_k, b_k; x) = \int_0^L d_k f_k(b_k; x)\phi_\gamma''(x)\phi_\delta''(x)dx \tag{19}$$

From the previous equation, the following bounds for $\Delta K_{\gamma\delta}$ are obtained

$$m_{\gamma\delta} d_k b_k \leq |\Delta K_{\gamma\delta}(d_k, b_k; x)| \leq M d_k b_k \tag{20}$$

being $m_{\gamma\delta} = \min_{x \in [0,L]}|\phi_\gamma''(x)\phi_\delta''(x)|$ and $M = \max_{x \in [0,L],\gamma,\delta}|\phi_\gamma''(x)\phi_\delta''(x)|$

Eq. (20) allows the introduction of an upper and a lower bound for Eq. (18), i.e.,

$$\left|\frac{\partial D_{ij}}{\partial r_h}\right| \geq \left|m_{\gamma\delta}\hat{H}_{i\gamma}\hat{H}_{j\delta}\left(d_k\frac{\partial b_k}{\partial r_h} + b_k\frac{\partial d_k}{\partial r_h}\right)\right|$$

$$\left|\frac{\partial D_{ij}}{\partial r_h}\right| \leq M\left|\sum_{\gamma\delta}\hat{H}_{i\gamma}\hat{H}_{j\delta}\left(d_k\frac{\partial b_k}{\partial r_h} + b_k\frac{\partial d_k}{\partial r_h}\right)\right|$$

$$\left|\frac{\partial D_{ij}}{\partial A_h}\right| \geq \left|m_{\gamma\delta}\hat{H}_{i\gamma}\hat{H}_{j\delta}\left(d_k\frac{\partial b_k}{\partial A_h} + b_k\frac{\partial d_k}{\partial A_h}\right)\right|$$

$$\left|\frac{\partial D_{ij}}{\partial A_h}\right| \leq M\left|\sum_{\gamma\delta}\hat{H}_{i\gamma}\hat{H}_{j\delta}\left(d_k\frac{\partial b_k}{\partial A_h} + b_k\frac{\partial d_k}{\partial A_h}\right)\right| \tag{21}$$

which is valid for every indices $i$, $j$ and $h$. In addition, still from Eq. (9), one obtains

$$\frac{\partial b_k}{\partial r_h} = \frac{\delta_k^h}{2}\sqrt{\frac{A_h}{r_h^3}}, \quad \frac{\partial b_k}{\partial A_h} = \frac{\delta_k^h}{2\sqrt{A_h r_h}},$$

$$\frac{\partial d_k}{\partial r_h} = \frac{\delta_k^h}{2}\sqrt{\frac{A_h}{r_h}}, \quad \frac{\partial d_k}{\partial A_h} = \frac{\delta_k^h}{2\sqrt{r_h^3 A_h}},$$

(22)

where $\delta_k^h$ is the Kronecker delta. Previous expressions allow Eq. (21) to be expressed in terms of damage shape $r_h$ and intensity $A_h$, e.g.,

$$\left|\frac{\partial D_{ij}}{\partial r_h}\right| \geq \frac{A_h}{r_h}\left|m_{\gamma\delta}\hat{H}_{i\gamma}\hat{H}_{j\delta}\right|$$

$$\left|\frac{\partial D_{ij}}{\partial r_h}\right| \leq M\frac{A_h}{r_h}\left|\sum_{\gamma\delta}\hat{H}_{i\gamma}\hat{H}_{j\delta}\right|$$

$$\left|\frac{\partial D_{ij}}{\partial A_h}\right| \geq \frac{1}{2}\left(1+\frac{1}{r_h^2}\right)\left|m_{\gamma\delta}\hat{H}_{i\gamma}\hat{H}_{j\delta}\right|$$

$$\left|\frac{\partial D_{ij}}{\partial A_h}\right| \leq \frac{M}{2}\left(1+\frac{1}{r_h^2}\right)\left|\sum_{\gamma\delta}\hat{H}_{i\gamma}\hat{H}_{j\delta}\right|$$

(23)

The function $\hat{D}_{ij}$ tends to a finite non-zero value as $A_h \to 0$; as a consequence, the following observations can be made:

(a) the sensitivity of $D_{ij}$ with respect to damage local shape $r_h$ vanishes linearly as $A_h$;

(b) the sensitivity of $D_{ij}$ with respect to damage intensity $A_h$ is strictly positive and bounded by a finite positive value. Indeed, Eq. (19) assures that the stiffness variation $\Delta K_{\gamma\delta}$ is strictly positive for $\gamma = \delta$, thus the norm infinity $\left\|m_{\gamma\delta}\hat{H}_{i\gamma}D_{\delta j}\right\|_\infty$ is greater than zero.

By passing to the limit in Eq. (23), the ratio between the sensitivities of $D$ can be evaluated

$$\lim_{\|A\|_\infty \to 0}\frac{\left\|\frac{\partial}{\partial r}D(A,r)\right\|_\infty}{\left\|\frac{\partial}{\partial A}D(A,r)\right\|_\infty} = 0$$

(24)